Analysis of AC link topologies in non-isolated DC/DC triple active bridge converter for current stress minimization

Hebala, Osama M.; Aboushady, Ahmed A.; Ahmed, Khaled H.

Published in:
2017 IEEE 6th International Conference on Renewable Energy Research and Applications (ICRERA)

DOI:
10.1109/ICRERA.2017.8191132

Publication date:
2017

Document Version
Author accepted manuscript

Analysis of AC link Topologies in Non-Isolated DC/DC Triple Active Bridge Converter for Current Stress Minimization

Osama M. Hebala
School of Engineering
Robert Gordon University
Scotland, UK
o.m.a.m.hebala@rgu.ac.uk
Arab Academy for Science, Technology and Maritime Transport (AASTMT),
Alexandria, Egypt

Ahmed A. Aboushady
School of Engineering and Built Environment
Glasgow Caledonian University
Glasgow, UK
ahmed.aboushady@gcu.ac.uk

Khaled H. Ahmed
Department of Electronic & Electrical Engineering, Faculty of Engineering, University of Strathclyde, UK
khaled.ahmed@ieee.org

***Abstract*— This paper presents analysis of the non-isolated DC/DC triple active bridge (TAB) converter under various purely inductor-based AC link topologies. The objective of the analysis is to find the topology that incorporates the least value of the AC link inductors which leads to reduced converter footprint in addition to minimum internal current stresses. Modelling of the TAB under each of the different topologies is presented in per unit expressions of power transfer and reactive power assuming fundamental harmonic analysis. The power expressions are used to calculate the inductor values necessary to achieve same rated power transfer of Dual Active Bridge (DAB) converter for the sake of standardizing comparison. On this basis, the topology requiring the least value of interface inductors, hence lowest footprint, is identified. Furthermore, based on phase shift control, particle swarm optimization (PSO) is used to calculate optimal phase shift ratios in each of the proposed topologies to minimize reactive power loss (hence current stress). The topology with minimum stresses is therefore identified and the results are substantiated using a Matlab-Simulink model to verify the theoretical analysis.**

Keywords— AC link, current stress, particle swarm optimization (PSO), reactive power, triple active bridge (TAB).

I. INTRODUCTION

The need for flexible energy management systems capable of capturing energy from diverse energy sources, and interfacing them with energy storage elements in a multi-directional power flow manner, is increasing. Possible applications include interface of fuel cell vehicles (FCVs) and hybrid electric vehicles (HEVs) [1], renewable energy sources in microgrids [2], and uninterruptible power supplies. The voltage-current characteristics of loads are usually different than those of energy sources and storage devices. Accordingly, multiport DC/DC converters became increasingly important to enable interface of sources, storages and loads.

Derived from the dual active bridge topology [3], multiport converters with AC link based on multi-winding transformer interface is suggested in [4-9]. In [4] harmonic fundamental analysis as well as the operating modes, based on duty-changed modulation, has been carried out for isolated triple active bridge. Authors in [5] proposed a duty ratio modulation to extend ZVS for the isolated the triple active bridge. Furthermore a control technique was designed to achieve voltage control, power flow management, and soft-switching for the TAB converter in a fuel cell and super capacitor system. However the proposed model in both [4] and [5] is not generalized as the duty ratio of one of the bridge voltages was assumed to be constant. A more generalized consideration of the isolated TAB phase shift control is introduced in [6] where a control technique is developed for operating TAB with low losses.

The use of the three-winding transformer in TAB often leads to higher copper as well as switching losses. This happens if two sources are providing ac voltages that are not in phase then their resulting flux oppose each other which decreases the resultant flux [10]. This will decrease the induced voltages of the transformer winding besides high inrush currents will flow through the converter as well as the transformer winding.

In this paper, a purely-inductor based AC link design is considered to study the non-isolated TAB converter. Absence of interface transformer in non-isolated converter can significantly reduce converter weight and footprint since inductors can be air-core based, avoids magnetic saturation, and mitigates the high frequency constraints imposed by high losses in magnetic cores.

The paper is organized in 6 sections. The AC link topologies under investigation in addition to the generalized steady state converter modelling are introduced in section 2. Section 3 includes the calculation of AC link inductors. This is followed by the study of the reactive power minimization of the TAB under the investigated AC link topologies in section 4. Matlab/Simulink TAB is presented in section 5, while section 6 concludes and summarises the main paper findings.

II. GENERIC TRIPLE ACTIVE BRIDGE MODELLING

A. Development of a generic TAB structure

Non-isolated TAB, composed of three front-to-front H-bridges is shown in Fig. 1. Equivalent circuit of the non-isolated TAB is shown in Fig. 2 and accordingly possible topologies of the AC link can be constructed as shown in Table I.

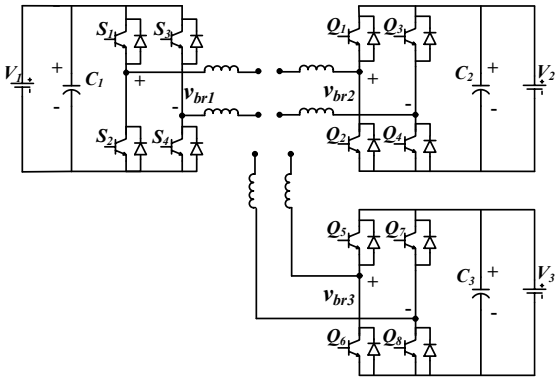

Fig 1. Circuit diagram of Triple Active Bridge (TAB)

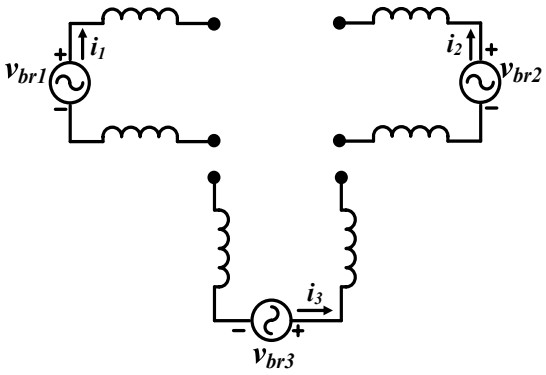

Fig 2. Equivalent circuit of the non-isolated TAB

TABLE I. Topologies for the AC link of the non-isolated TAB

Topology 1	Topology 2	Topology 3
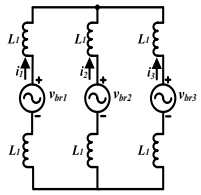	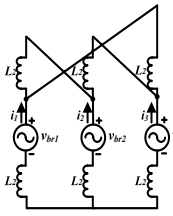	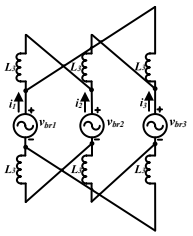
Topology 4	**Topology 5**	**Topology 6**
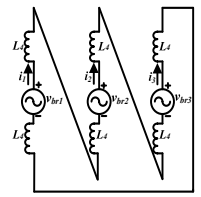	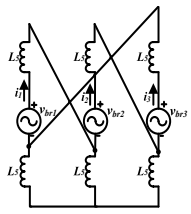	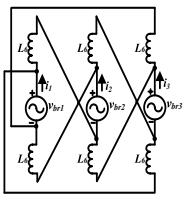

B. Steady State Converter Modelling

Fig. 3 shows typical AC voltage waveforms at the three active bridges. D_1, D_2 and D_3 are the three duty ratios of the three bridge voltages V_{br1}, V_{br2} and V_{br3} respectively; such that $0 \le D_1 \le 1, 0 \le D_2 \le 1, 0 \le D_3 \le 1$.
In addition, D_{12} signifies the phase shift between the positive-going edges of V_{br1} and V_{br2}, and similarly D_{13} indicates the phase shift between the positive-going edges of V_{br1} and V_{br3}; such that $-0.5 \le D_{12} \le 0.5$, $-0.5 \le D_{13} \le 0.5$. Equations (1)-(3) show the fundamental harmonic expressions for the bridge voltages in per unit normalized to the base voltage V_1. Accordingly, K_{12} represents the voltage conversion gain between bridges 1 and 2; and K_{13} represents the voltage gain between bridges 1 and 3. This paper covers the unity gain mode case where the three DC voltage levels are equal (i.e. K_{12}=1 and K_{13}=1) which could be particularly relevant in applications where the main objective of the TAB converter is power flow regulation between the three DC sources.

$$v_{br1}(t) = V_{1\,max}\, sin(\omega t - \delta_1) \quad (1)$$
$$v_{br2}(t) = V_{2\,max}\, sin(\omega t - \delta_2) \quad (2)$$
$$v_{br3}(t) = V_{3\,max}\, sin(\omega t - \delta_3) \quad (3)$$

Such that

$$V_{1\,max} = \frac{4}{\pi} sin\left(\frac{D_1 * \pi}{2}\right)$$

$$V_{2\,max} = \frac{4K_{12}}{\pi} sin\left(\frac{D_2 * \pi}{2}\right)$$

$$V_{3\,max} = \frac{4K_{13}}{\pi} sin\left(\frac{D_3 * \pi}{2}\right)$$

Where, $K_{12} = \frac{V_2}{V_1}$, $K_{13} = \frac{V_3}{V_1}$

$$\delta_1 = 0,\ \delta_2 = \pi(D_{12} + \frac{D_2 - D_1}{2})$$

$$\delta_3 = \pi(D_{13} + \frac{D_3 - D_1}{2})$$

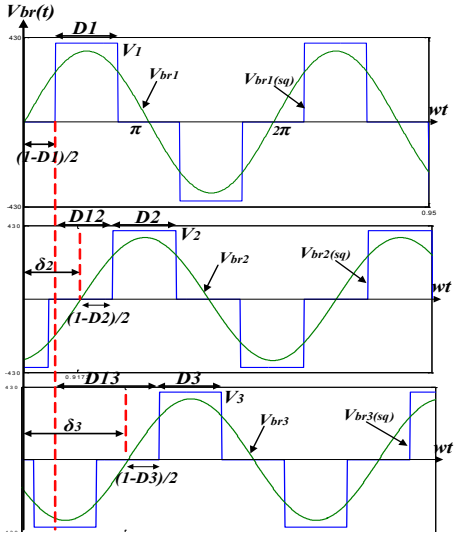

Fig 3. Definition of phase shift control ratios for the three active bridges

TABLE II. Per Unit Active/Reactive Power at Each Bridge Normalized to P_{base}

Topology		Active/Reactive power expression
1	P_1	$\frac{4L_{base}}{3\pi L_1} V_{1\,rms}\,(\,V_{2\,rms}\,\sin(\delta_2) + V_{3\,rms}\,\sin(\delta_3)\,)$
	Q_1	$\frac{4L_{base}}{3\pi L_1} V_{1\,rms}\,(\,2V_{1\,rms} - V_{2\,rms}\,\cos(\delta_2) - V_{3\,rms}\,\cos(\delta_3)\,)$
	P_2	$\frac{4L_{base}}{3\pi L_1} V_{2\,rms}\,(cos(\delta_2)[-2V_{2\,rms}\,\sin(\delta_2) + V_{3\,rms}\,\sin(\delta_3)\,] - sin(\delta_2)[\,V_{1\,rms} - 2V_{2\,rms}\,\cos(\delta_2) + V_{3\,rms}\cos(\delta_3)])$
	Q_2	$-\frac{4L_{base}}{3\pi L_1} V_{2\,rms}\,(sin(\delta_2)[-2V_{2\,rms}\,\sin(\delta_2) + V_{3\,rms}\,\sin(\delta_3)\,] + cos(\delta_2)[\,V_{1\,rms} - 2V_{2\,rms}\,\cos(\delta_2) + V_{3\,rms}\cos(\delta_3)])$
	P_3	$\frac{4L_{base}}{3\pi L_1} V_{3\,rms}\,(cos(\delta_3)[V_{2\,rms}\,\sin(\delta_2) - 2\,V_{3\,rms}\,\sin(\delta_3)\,] - sin(\delta_3)[\,V_{1\,rms} + V_{2\,rms}\,\cos(\delta_2) - 2\,V_{3\,rms}\cos(\delta_3)])$
	Q_3	$-\frac{4L_{base}}{3\pi L_1} V_{3\,rms}\,(sin(\delta_3)[V_{2\,rms}\,\sin(\delta_2) - 2\,V_{3\,rms}\,\sin(\delta_3)] + cos(\delta_3)[\,V_{1\,rms} + V_{2\,rms}\,\cos(\delta_2) - 2\,V_{3\,rms}\cos(\delta_3)])$
2	P_1	$\frac{2L_{base}}{\pi L_2} V_{1\,rms}\,(\,0.5V_{2\,rms}\,\sin(\delta_2) + 0.5V_{3\,rms}\,\sin(\delta_3)\,)$
	Q_1	$\frac{2L_{base}}{\pi L_2} V_{1\,rms}\,(\,V_{1\,rms} - 0.5V_{2\,rms}\,\cos(\delta_2) - 0.5V_{3\,rms}\,\cos(\delta_3)\,)$
	P_2	$\frac{2L_{base}}{\pi L_2} V_{2\,rms}\,(cos(\delta_2)[-V_{2\,rms}\,\sin(\delta_2) + 0.5\,V_{3\,rms}\,\sin(\delta_3)] - sin(\delta_2)[\,0.5V_{1\,rms} - V_{2\,rms}\,\cos(\delta_2) + 0.5V_{3\,rms}\,\cos(\delta_3)])$
	Q_2	$-\frac{2L_{base}}{\pi L_2} V_{2\,rms}\,(sin(\delta_2)[-V_{2\,rms}\,\sin(\delta_2) + 0.5\,V_{3\,rms}\,\sin(\delta_3)] + cos(\delta_2)[\,0.5V_{1\,rms} - V_{2\,rms}\,\cos(\delta_2) + 0.5V_{3\,rms}\,\cos(\delta_3)])$
	P_3	$\frac{2L_{base}}{\pi L_2} V_{3\,rms}\,(cos(\delta_3)[\,0.5V_{2\,rms}\,\sin(\delta_2) - V_{3\,rms}\,\sin(\delta_3)] - sin(\delta_3)[\,0.5V_{1\,rms} + 0.5V_{2\,rms}\,\cos(\delta_2) - 0.5V_{3\,rms}\,\cos(\delta_3)])$
	Q_3	$-\frac{2L_{base}}{\pi L_2} V_{3\,rms}\,(sin(\delta_3)[\,0.5V_{2\,rms}\,\sin(\delta_2) - V_{3\,rms}\,\sin(\delta_3)] + cos(\delta_3)[\,0.5V_{1\,rms} + 0.5V_{2\,rms}\,\cos(\delta_2) - 0.5V_{3\,rms}\,\cos(\delta_3)])$
3	P_1	$\frac{2L_{base}}{\pi L_3} V_{1\,rms}\,(\,V_{2\,rms}\,\sin(\delta_2) + V_{3\,rms}\,\sin(\delta_3)\,)$
	Q_1	$\frac{2L_{base}}{\pi L_3} V_{1\,rms}\,(\,2\,V_{1\,rms} - V_{2\,rms}\,\cos(\delta_2) - V_{3\,rms}\,\cos(\delta_3)\,)$
	P_2	$\frac{2L_{base}}{\pi L_3} V_{2\,rms}\,(cos(\delta_2)[\,-2V_{2\,rms}\,\sin(\delta_2) + V_{3\,rms}\,\sin(\delta_3)] - sin(\delta_2)[\,V_{1\,rms} - 2V_{2\,rms}\,\cos(\delta_2) + V_{3\,rms}\,\cos(\delta_3)])$
	Q_2	$-\frac{2L_{base}}{\pi L_3} V_{2\,rms}\,(sin(\delta_2)[\,-2V_{2\,rms}\,\sin(\delta_2) + V_{3\,rms}\,\sin(\delta_3)] + cos(\delta_2)[\,V_{1\,rms} - 2V_{2\,rms}\,\cos(\delta_2) + V_{3\,rms}\,\cos(\delta_3)])$
	P_3	$\frac{2L_{base}}{\pi L_3} V_{3\,rms}\,(cos(\delta_3)[\,V_{2\,rms}\,\sin(\delta_2) - 2V_{3\,rms}\,\sin(\delta_3)] - sin(\delta_3)[\,V_{1\,rms} + V_{2\,rms}\,\cos(\delta_2) - 2V_{3\,rms}\,\cos(\delta_3)])$
	Q_3	$-\frac{2L_{base}}{\pi L_3} V_{3\,rms}\,(sin(\delta_3)[\,V_{2\,rms}\,\sin(\delta_2) - 2V_{3\,rms}\,\sin(\delta_3)] + cos(\delta_3)[\,V_{1\,rms} + V_{2\,rms}\,\cos(\delta_2) - 2V_{3\,rms}\,\cos(\delta_3)])$
4	P_1	$\frac{4L_{base}}{3\pi L_4} V_{1\,rms}\,(\,V_{2\,rms}\,\sin(\delta_2) + V_{3\,rms}\,\sin(\delta_3))$
	Q_1	$\frac{4L_{base}}{3\pi L_4} V_{1\,rms}\,(\,V_{1\,rms} - V_{2\,rms}\,\cos(\delta_2) - V_{3\,rms}\,\cos(\delta_3))$
	P_2	$-\frac{4L_{base}}{3\pi L_4} V_{2\,rms}\,(cos(\delta_2)\,[\,V_{2\,rms}\,\sin(\delta_2) + V_{3\,rms}\,\sin(\delta_3)] + sin(\delta_2)[\,V_{1\,rms} - V_{2\,rms}\,\cos(\delta_2) - V_{3\,rms}\cos(\delta_3)])$
	Q_2	$\frac{4L_{base}}{3\pi L_4} V_{2\,rms}\,(sin(\delta_2)\,[\,V_{2\,rms}\,\sin(\delta_2) + V_{3\,rms}\,\sin(\delta_3)] - cos(\delta_2)[\,V_{1\,rms} - V_{2\,rms}\,\cos(\delta_2) - V_{3\,rms}\cos(\delta_3)])$
	P_3	$-\frac{4L_{base}}{3\pi L_4} V_{3\,rms}\,(cos(\delta_3)\,[\,V_{2\,rms}\,\sin(\delta_2) + V_{3\,rms}\,\sin(\delta_3)]\,) + sin(\delta_3)[\,V_{1\,rms} - V_{2\,rms}\,\cos(\delta_2) - V_{3\,rms}\cos(\delta_3)])$
	Q_3	$\frac{4L_{base}}{3\pi L_4} V_{3\,rms}\,(sin(\delta_3)\,[\,V_{2\,rms}\,\sin(\delta_2) + V_{3\,rms}\,\sin(\delta_3)]\,) - cos(\delta_3)[\,V_{1\,rms} - V_{2\,rms}\,\cos(\delta_2) - V_{3\,rms}\cos(\delta_3)])$
5	P_1	$\frac{4L_{base}}{\pi L_5} V_{1\,rms}\,(-0.25V_{2\,rms}\,\sin(\delta_2) - 0.25\,V_{3\,rms}\,\sin(\delta_3))$
	Q_1	$\frac{4L_{base}}{\pi L_5} V_{1\,rms}\,(\,0.5V_{1\,rms} + 0.25V_{2\,rms}\,\cos(\delta_2) + 0.25\,V_{3\,rms}\cos(\delta_3))$
	P_2	$\frac{4L_{base}}{\pi L_5} V_{2\,rms}\,(cos(\delta_2)\,[-V_{2\,rms}\,\sin(\delta_2) - 0.5\,V_{3\,rms}\,\sin(\delta_3)]) + sin(\delta_2)[\,0.5V_{1\,rms} + V_{2\,rms}\,\cos(\delta_2) + 0.5\,V_{3\,rms}\cos(\delta_3)])$
	Q_2	$-\frac{4L_{base}}{\pi L_5} V_{2\,rms}\,(sin(\delta_2)\,[-V_{2\,rms}\,\sin(\delta_2) - 0.5\,V_{3\,rms}\,\sin(\delta_3)]) - cos(\delta_2)[\,0.5V_{1\,rms} + V_{2\,rms}\,\cos(\delta_2) + 0.5\,V_{3\,rms}\cos(\delta_3)])$
	P_3	$\frac{4L_{base}}{\pi L_5} V_{3\,rms}\,(cos(\delta_3)\,[-0.5V_{2\,rms}\,\sin(\delta_2) - V_{3\,rms}\,\sin(\delta_3)] + sin(\delta_3)[\,0.5V_{1\,rms} + 0.5V_{2\,rms}\,\cos(\delta_2) + V_{3\,rms}\cos(\delta_3)])$
	Q_3	$-\frac{4L_{base}}{\pi L_5} V_{3\,rms}\,(sin(\delta_3)\,[-0.5V_{2\,rms}\,\sin(\delta_2) - V_{3\,rms}\,\sin(\delta_3)] - cos(\delta_3)[\,0.5V_{1\,rms} + 0.5V_{2\,rms}\,\cos(\delta_2) + V_{3\,rms}\cos(\delta_3)])$
6	P_1	$\frac{4L_{base}}{\pi L_6} V_{1\,rms}\,(-0.5V_{2\,rms}\,\sin(\delta_2) - 0.5V_{3\,rms}\,\sin(\delta_3))$
	Q_1	$\frac{4L_{base}}{\pi L_6} V_{1\,rms}\,(\,V_{1\,rms} + 0.5V_{2\,rms}\,\cos(\delta_2) + 0.5V_{3\,rms}\,\cos(\delta_3))$
	P_2	$\frac{4L_{base}}{\pi L_6} V_{2\,rms}\,(cos(\delta_2)\,[\,-V_{2\,rms}\,\sin(\delta_2) - 0.5V_{3\,rms}\,\sin(\delta_3)]) - sin(\delta_2)[-0.5V_{1\,rms} - V_{2\,rms}\,\cos(\delta_2) - 0.5V_{3\,rms}\,\cos(\delta_3)])$
	Q_2	$-\frac{4L_{base}}{\pi L_6} V_{2\,rms}\,(sin(\delta_2)\,[\,-V_{2\,rms}\,\sin(\delta_2) - 0.5V_{3\,rms}\,\sin(\delta_3)]) + cos(\delta_2)[-0.5V_{1\,rms} - V_{2\,rms}\,\cos(\delta_2) - 0.5V_{3\,rms}\,\cos(\delta_3)])$
	P_3	$\frac{4L_{base}}{\pi L_6} V_{3\,rms}\,(cos(\delta_3)\,[-0.5V_{2\,max}\,\sin(\delta_2) - V_{3\,max}\,\sin(\delta_3)]) - sin(\delta_3)[-0.5V_{1\,rms} - 0.5V_{2\,rms}\,\cos(\delta_2) - V_{3\,rms}\,\cos(\delta_3)])$
	Q_3	$-\frac{4L_{base}}{\pi L_6} V_{3\,rms}\,(sin(\delta_3)\,[-0.5V_{2\,max}\,\sin(\delta_2) - V_{3\,max}\,\sin(\delta_3)]) + cos(\delta_3)[-0.5V_{1\,rms} - 0.5V_{2\,rms}\,\cos(\delta_2) - V_{3\,rms}\,\cos(\delta_3)])$

The currents at each bridge i_n (n=1, 2, 3), for the investigated topologies shown in Table I, are derived using basic circuit analysis based on the fundamental harmonic approximation from the voltage expressions (1)-(3). The bridge currents are calculated in per unit using I_{base} that is derived from P_{max} of Dual Active Bridge (DAB) [3, 11]. The base current is defined as,

$$I_{base} = \frac{V_{base}}{Z_{base}} \tag{4}$$

Such that; $V_{base} = V_1$ and $Z_{base} = 8fL_{base}$

Where f is the switching frequency

Therefore,

$$P_{base} = \frac{{V_{base}}^2}{Z_{base}} \tag{5}$$

Consequently, per unit active and reactive power expressions at each bridge for all topologies are calculated by (6) and (7) and are shown in Table II.

$$P_n = 0.5\,V_{\boldsymbol{n}\,max}\;I_{\boldsymbol{n}\,max}\;cos(\delta_{\boldsymbol{n}} - \theta_{i_{\boldsymbol{n}}}) \tag{6}$$

$$Q_n = 0.5\,V_{n\,max}\;I_{n\,max}\;sin(\delta_n - \theta_{i_n}) \tag{7}$$

Where,

n is the number of the bridge and θ_{i_n} the angle of the current i_n

The per unit expressions of active power are calculated at unity gain mode case where the three DC voltage levels are equal (i.e. K_{12}=1 and K_{13}=1). In addition, these expressions are function of D_1, D_2, D_3, D_{12} and D_{13} such that

$$V_{n\,rms} = \frac{4}{\pi\sqrt{2}} sin\left(\frac{D_n * \pi}{2}\right) \tag{8}$$

$$\delta_n = \pi(D_{1n} + \frac{D_n - D_1}{2}) \tag{9}$$

Where,

n is the number of the bridge (n=1, 2, 3)

III. Calculation and Comparison of AC Link Topologies's Inductor

The objective of the analysis in this section is to calculate the value of L_n for each topology in Table I that would ensure a max power transfer of 1pu. The procedure is to equate active power at bridge 1 (P_1) to maximum power (P_n =1pu) and substitute with the duty ratios D_1=D_2=D_3=1 and phase shift ratios D_{12}=D_{13}=0.5 then solve to get L_n as a function of L_{base}. The inductor value for the AC link for each topology is shown in Table IIII.

TABLE III. Inductor values of the TAB AC link topologies

Topology (1)	Topology (2)	Topology (3)
$L_1 = \frac{4^3}{6\pi^3} L_{base}$	$L_2 = \frac{4^3}{4\pi^3} L_{base}$	$L_3 = \frac{4^3}{2\pi^3} L_{base}$
Topology (4)	**Topology (5)**	**Topology (6)**
$L_4 = \frac{4^3}{6\pi^3} L_{base}$	$L_5 = \frac{4^3}{4\pi^3} L_{base}$	$L_6 = \frac{4^3}{2\pi^3} L_{base}$

L_{base} is defined as the equivalent interface inductor in the DAB converter, as shown in Fig. 4. The value of L_{base} is calculated at maximum power transfer which is obtained with 90º phase shift between bridge voltages [3, 11], as stated in (10). The maximum power transfer is assumed to be 1pu.

$$P_{max} = \frac{V_{br1}\, V_{br2}}{8\, f\, L_{base}} \tag{10}$$

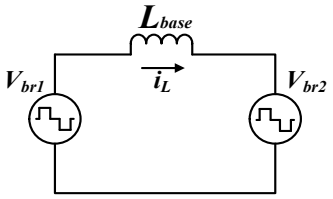

Fig. 4. DAB AC equivalent circuit

Based on the inductor value of the AC link for each topology shown in Table III, Topologies 1 and 4 is noticed to have minimum inductor values. This means that these two topologies can transfer the full range of power with the least AC link's inductor value.

IV. Reactive Power Minimization Using PSO

After the calculation of the inductor values for each topology which ensure a maximum power transfer of 1pu, it is now necessary to investigate the topology that minimizes the total reactive power loss (and hence current stresses) for the same level of power transferred in the topologies under study. To perform this, different scenarios for power transfer at the bridges are selected by equating the power equations P_n to such values and then particle swarm optimization (PSO) [12] is used, with the power at the bridges as equality constraints, to minimize total reactive power loss $Q_{tot}=Q_1+Q_2+Q_3$ where Q_n is calculated from (7) and shown in Table II.

A. Formulation of the minimization problem

The reactive power minimization for the TAB can be realized by calculating optimal phase shift ratios while achieving required power level at each bridge. This can be formulated as a multi-constrained minimization problem. The ranges of the control parameters (D_1, D_2, D_3, D_{12} and D_{13}) are considered to be the first constraint. Whereas the second constraint is set to be the required power transfer of each bridge.

The minimization objective is the total reactive power loss in the TAB converter. Minimizing the reactive power will lead to reducing the current stresses hence the conduction losses, which are considered to be the dominant portion of losses as discussed in [13].The objective function to be minimized is stated in (11) while the dimension space of the problems is composed of the five variables D_1, D_2, D_3, D_{12} and D_{13}. The proposed minimization technique is expressed as follows.

Minimize

$$Obj.Fun. = Q_{tot} \tag{11}$$

Where,

$Q_{tot} = Q_1 + Q_2 + Q_3$

Such that Q_n is calculated using (7), (See Table II)

Subject to

Equality constraint

P_n where n=1, 2, 3 (See Table II)

And the inequality constraint

$0 \le D_1 \le 1$, $0 \le D_2 \le 1$,$0 \le D_3 \le 1$

$-0.5 \le D_{12} \le 0.5$, $-0.5 \le D_{13} \le 0.5$

B. Optimization Tool

Particle swarm optimization (PSO) method is chosen to be applied to the TAB under each of the investigated AC link topologies to calculate the optimal phase ratios. The PSO method encompasses two model equations [12]. The first one represent the velocity of each particle in the N-dimensional space. The velocity depends on three parameters: the previous velocity, personal experience of the particle and the global experience of the whole swarm, as in (12). While the second equation is responsible for updating the position of each particle depending on the previous position and the current velocity (13). Fig. 5 shows the flow diagram illustrating the principle of operation of the PSO.

$$V_i^{m+1} = w\, V_i^m + c_1 r_1 (Pbest_i^m - X_i^m) + c_2 r_2 (gbest_i^m - X_i^m) \tag{12}$$

$$X_i^{m+1} = X_i^m + V_i^{m+1} \tag{13}$$

Where

- m is the iteration index.
- c_1 and c_2 are two positive constants, both set equal 2.
- r_1 and r_2 are two randomly generated numbers, such that $0 \le r_1 \le 1$, $0 \le r_2 \le 1$
- w is the inertia constant, such that w=0.9-(0.005*m).
- $pbest_i^m$ is the best position particle i achieved based on its own experience ;

$$Pbest_i^m = [X_{i1}^{Pbest}, X_{i2}^{Pbest}, \dots, X_{iN}^{Pbest}]$$

- $gbest^m$ is the best position based on overall swarm's experience.

Each individual (particle) of the swarm, in this problem, consists of a five values which are D_1, D_2, D_3, D_{12} and D_{13}. The PSO-based algorithm, in each iteration of the iterative loop, is supposed to search for the optimal phase shifts to achieve the minimum total reactive power while simultaneously maintain the required power level at each bridge.

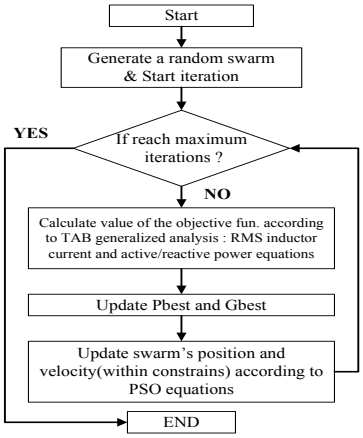

Fig. 5. Main flow chart of PSO

The Matlab m-file software has been used as the platform for the off-line PSO application to the TAB for all investigated topologies. The per unit TAB model discussed in previous sections has been used as the basis of the PSO-offline application. The simulation was carried out for unity gain operating mode where $K_{12}=K_{13}=1$.

C. Steady State Results

The steady state per unit total reactive losses and RMS current stresses at selected sets of power levels after the offline application of the PSO are presented in Table IV and Table V. The shown per unit results are based on the base values stated in Table VI.

TABLE IV. Steady State Results of offline PSO at P_1=-0.6pu ,P_2=0.1pu, P_3=0.5pu

Topology	Q_{tot} (pu)	I_1 (pu)	I_2 (pu)	I_3 (pu)
1	0.4096	0.6732	0.1592	0.5285
2	0.4113	0.6751	0.1638	0.5278
3	0.4120	0.6746	0.1598	0.5310
4	0.6613	0.6387	0.6387	0.6387
5	2.2134	1.1310	1.2251	1.3269
6	2.2150	1.1405	1.2245	1.3208

TABLE V. Steady State Results of offline PSO at P_1=0.8pu,P_2=-0.5pu, P_3=-0.3pu

Topology	Q_{tot} (pu)	I_1 (pu)	I_2 (pu)	I_3 (pu)
1	0.7558	0.9550	0.5914	0.3697
2	0.7556	0.9567	0.5826	0.3789
3	0.7562	0.9561	0.5811	0.3699
4	1.2016	0.8609	0.8609	0.8609
5	2.4892	1.1685	1.2942	1.2968
6	2.5112	1.1810	1.2820	1.2953

TABLE VI. BASE VALUES

Parameter	Value
Base Voltage	192 Volt
L_{base}	0.25 mH
Base Current	48 Amp
Full-load power/Base Bower	9216 W

The total reactive power values as well as the bridge currents at each bridge presented in Table IV and Table V show that topology 1, 2 and 3 realize minimum reactive power and current stresses.

V. SIMULATION

Topology 1 can be identified to be the best topology through the inspection of Tables III, IV and V. This is due to the fact that it realizes both minimum AC link inductance as well as minimum reactive losses.

The analytical model for topology 1 of TAB was verified by a detailed simulation model of the converter using Simulink platform. Simulation parameters used are given in Table VII. The TAB converter was run with unity duty ratio of the three bridge voltages (i.e. $D_1=D_2=D_3=1$) and the full range of phase shifts D_{12} and D_{13} (i.e. $-0.5 \leqslant D_{12} \leqslant 0.5$ and $0.5 \leqslant D_{13} \leqslant 0.5$) was examined.

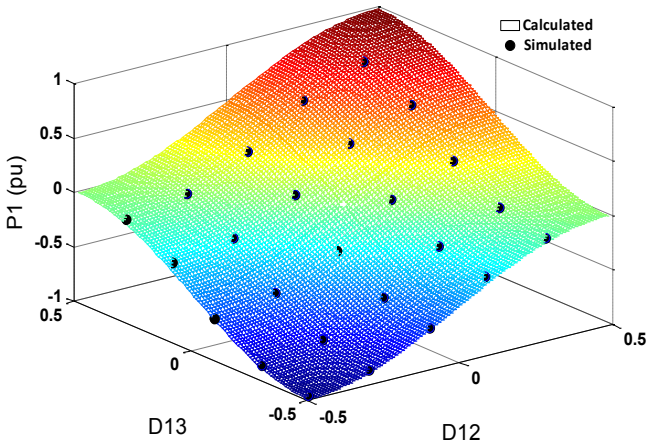

Fig. 6(a) Active Power at bridge 1: simulated vs calculated

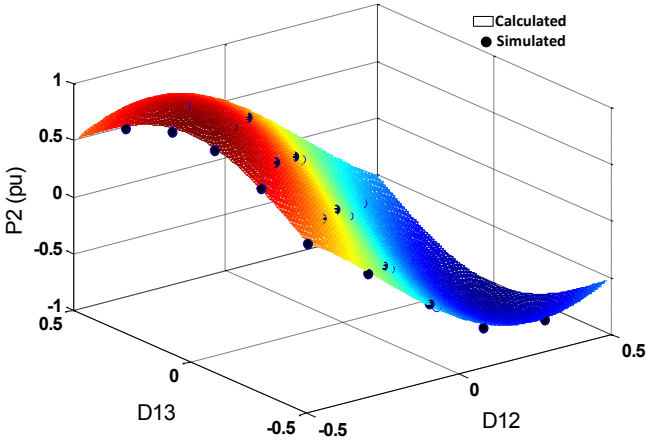

Fig. 6(b). Active Power at bridge 2: simulated vs calculated

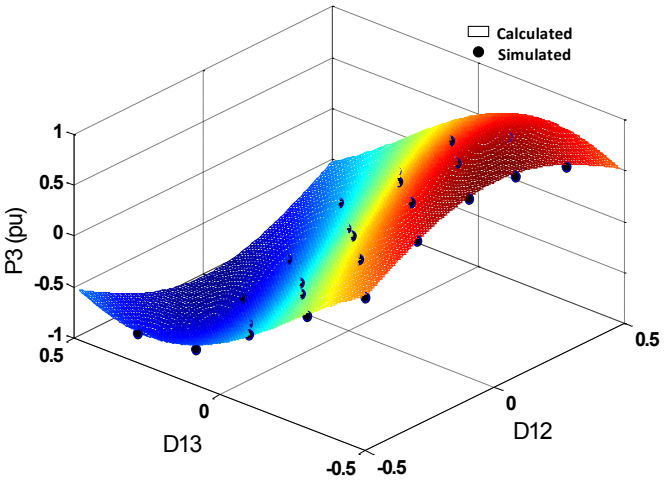

Fig. 6(c). Active Power at bridge 3: simulated vs calculated

Figs. 6 parts (a) to (c) show P_1, P_2 and P_3 achieved from simulation and from fundamental frequency analytical model closely matching while Fig. 6(d) confirms the accuracy of the total reactive power expressions. All presented results from simulation are in per unit with respect to the base values shown in Table VI. The plots show that the calculated model achieves an accepted level of accuracy and proves that the conclusions based on the analytical model can be adopted.

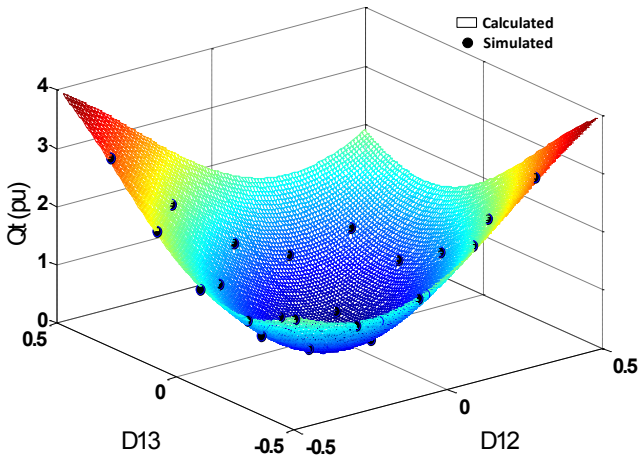

Fig. 6(d). Total Reactive Power: simulated vs calculated

TABLE VII. OPERATIONAL VALUES FOR THE SIMULATION

Parameter	Value
DC Voltage of 1st Bridge $\mathbf{V_1}$	192 Volt
DC Voltage of 2nd Bridge $\mathbf{V_2}$	192 Volt
DC Voltage of 3nd Bridge $\mathbf{V_3}$	192 Volt
Switching Frequency f_{sw}	2000 Hz
AC Link Interface inductor L	0.172 m H

VI. CONCLUSION

Per unit modelling and power flow analysis have been developed and investigated for non-isolated triple active bridge (TAB). The analyses were carried out for the TAB under various purely-inductive AC link topologies. The value of the AC link inductor was calculated for each topology to investigate the topology with the least inductor, hence least converter footprint. PSO was used to minimize reactive power losses for sets of power transfer scenario under all topologies. The first proposed topology has proven to achieve the best performance among other topologies, in terms of least AC link inductance required and least reactive power loss.

REFERENCES

[1] U. R. Prasanna and A. K. Rathore, "Dual Three-Pulse Modulation-Based High-Frequency Pulsating DC Link Two-Stage Three-Phase Inverter for Electric/Hybrid/Fuel Cell Vehicles Applications," in IEEE Journal of Emerging and Selected Topics in Power Electronics, vol. 2, no. 3, pp. 477-486, Sept. 2014.

[2] M. B. Udhyami and A. Mohan, "Multiple — Input bidirectional DC-DC power converter with renewable energy source," 2016 International Conference on Electrical, Electronics, and Optimization Techniques (ICEEOT), Chennai, 2016, pp. 1739-1744.

[3] R. W. A. A. De Doncker, D. M. Divan, and M. H. Kheraluwala, "A three-phase soft-switched high-power-density DC/DC converter for high-power applications," *IEEE Trans. Ind. Appl.*, vol. 27, no. 1, pp. 63–73, Jan. 1991.

[4] R. Yapa and A. Forsyth, "Extended soft switching operation of the triple active bridge convereter," *6th IET International Conference on Power Electronics, Machines and Drives (PEMD 2012)*, Bristol, 2012, pp. 1-6.

[5] H. Tao, A. Kotsopoulos, J. L. Duarte and M. A. M. Hendrix, "Transformer-Coupled Multiport ZVS Bidirectional DC–DC Converter With Wide Input Range," in *IEEE Transactions on Power Electronics*, vol. 23, no. 2, pp. 771-781, March 2008.

[6] Chuanhong Zhao, S. D. Round, and J. W. Kolar, "An Isolated Three-Port Bidirectional DC-DC Converter With Decoupled Power Flow Management," IEEE Transactions on Power Electronics, vol. 23, no. 5, pp. 2443-2453, Sept. 2008.

[7] V. N. S. R. Jakka and A. Shukla, "A triple port active bridge converter based multi-fed power electronic transformer," 2016 IEEE Energy Conversion Congress and Exposition (ECCE), Milwaukee, WI, 2016, pp. 1-8.

[8] G. Zhigang and J. Fenlin, "Isolated multi-port DC-DC converter based on a high frequency transformer," 2015 18th International Conference on Electrical Machines and Systems (ICEMS), Pattaya, 2015, pp. 564-568.

[9] Q. Mei, Xu Zhen-lin and W. y. Wu, "A novel multi-port DC-DC converter for hybrid renewable energy distributed generation systems connected to power grid," 2008 IEEE International Conference on Industrial Technology, Chengdu, 2008, pp. 1-5.

[10] V. N. S. R. Jakka, A. Shukla and G. D. Demetriades, "Dual-Transformer-Based Asymmetrical Triple-Port Active Bridge (DT-ATAB) Isolated DC–DC Converter," in *IEEE Transactions on Industrial Electronics*, vol. 64, no. 6, pp. 4549-4560, June 2017.

[11] Krismer, F.; Kolar, J.W.; "Closed Form Solution for Minimum Conduction Loss Modulation of DAB Converters," Power Electronics, IEEE Transactions on, vol.27, no.1, pp.174-188, Jan. 2012.

[12] J. Kennedy and R. Eberhart, "Particle swarm optimization," Neural Networks, 1995. Proceedings, IEEE International Conference on, Perth, WA, 1995, pp. 1942-1948 vol.4.

[13] S. Inoue and H. Akagi, "A Bidirectional DC–DC Converter for an Energy Storage System With Galvanic Isolation," in IEEE Transactions on Power Electronics, vol. 22, no. 6, pp. 2299-2306, Nov. 2007.